

Polymer-Derived Ceramic Aerogels to Immobilize Sulfur for Li-S Batteries

Andrea Zambotti, Fangmu Qu,* Giacomo Costa, Magdalena Graczyk-Zajac, and Gian Domenico Sorarù

Lithium–sulfur batteries are among the promising high-capacity candidates owing to the superior theoretical capacity of sulfur, when compared with conventional cathodes such as LiCoO_2 . However, several issues must be addressed before these batteries can be considered fully operational. Major issues regard the insulating nature of sulfur and the so-called shuttle effect of soluble polysulfides, which dramatically reduces the cathode capacity upon cycling. Herein, three carbon-containing polymer-derived ceramic aerogels are characterized belonging to the Si-C-O and Si-C-N systems, infiltrated with sulfur to work as cathodes for Li-S batteries. The electrochemical performances are evaluated in relation to the microstructural and chemical features of such materials. In particular, the effect of the pore size of the ceramic matrices on the shuttling behavior of polysulfides is investigated. Despite the high initial specific capacities exceeding hundreds of mAh g^{-1} , all types of cathodes show stable capacities in the 60–120 mAh g^{-1} range after 100 cycles.

1. Introduction

As demonstrated in the pioneering work of Yajima in the mid-70s, nonoxide ceramics such as SiC can be obtained via pyrolysis of Si-containing preceramic polymers.^[1] Since then, the so-called polymer-derived ceramic (PDC) route has been demonstrated for a large number of binary (Si-C; B-N), ternary (Si-C-O, Si-C-N), and quaternary (Si-B-C-O; Si-B-C-N, Si-Ti-O-C) ceramic compositions.^[2–4] The PDC route also allows processing components with difficult-to-obtain microstructure and/or shape: fibers,^[5] foams,^[6] aerogels,^[7] and microlattices/honeycombs.^[8]

Taking advantage of the high chemical and thermal stability of PDC aerogels and from their easy tailorable composition and porosity (i.e., total porosity and pore size),^[9,10] they have been proposed for different applications like matrices for thermal energy storage (TES) to confine high temperature melting and chemically aggressive phase change materials (PCM)^[11,12] or as sorbents for water purification.^[13,14] Polymer-derived silicon oxycarbides have also shown higher lithium storage capacity compared to conventional graphite-based anodes^[15] and SiOC aerogels displayed also very high lithium reversible capacity at very high charging/discharging rates, namely, 300 mAh g^{-1} at 20 C.^[16]


Nowadays lithium-ion batteries are used in portable electronics and cars and are proposed as backup storage for many intermittent renewable energy sources.^[17,18] However, researchers are still working to improve the performance of these devices either to increase the specific capacity or by substituting rare and health-hazardous elements, like Co present in most of the cathode materials, with safer ones. A possible solution to these problems is to use sulfur as cathode material in Li-S batteries.^[19] Sulfur has a higher theoretical specific capacity, 1,675 mAh g^{-1} compared to 150–220 mAh g^{-1} for common cathode materials, it is nontoxic, abundant, and available on the earth's crust. However, sulfur cathodes suffer from other problems: sulfur is electrically insulating and shows a rapid capacity fading related to the high solubility of lithium polysulfides in the liquid electrolyte which results in the well-known “shuttle effect.” Moreover, during the lithiation, the volume of sulfur increases by around 80%, leading to electrode disintegration during cycling.^[20] To overcome these limitations, sulfur is often confined in a conductive C-based matrix. Based on the idea that porosity also plays a pivotal role in blocking or reducing the diffusion of

A. Zambotti, G. Costa, G. D. Sorarù
Department of Industrial Engineering
Glass & Ceramics Laboratory
University of Trento
Via Sommarive 9, 38123 Trento, Italy

F. Qu, M. Graczyk-Zajac
Institute of Materials Science Darmstadt University of Technology
Otto-Berndt-Str. 3, 64287 Darmstadt, Germany
E-mail: fangmu.qu@stud.tu-darmstadt.de

M. Graczyk-Zajac
Research and Development
EnBW Energie Baden-Württemberg AG
Durlacher Allee 93, 76131 Karlsruhe, Germany

G. D. Sorarù
National Research Council of Italy (ICMATE-CNR)
Institute of Condensed Matter Chemistry and Technologies for Energy
Via Marini 6, I-16149 Genoa, Italy

 The ORCID identification number(s) for the author(s) of this article can be found under <https://doi.org/10.1002/ente.202300488>.

© 2020 The Authors. Energy Technology published by Wiley-VCH GmbH. This is an open access article under the terms of the Creative Commons Attribution-NonCommercial-NoDerivs License, which permits use and distribution in any medium, provided the original work is properly cited, the use is non-commercial and no modifications or adaptations are made.

DOI: 10.1002/ente.202300488

lithium polysulfides from the cathode to the anode, many different forms of porous carbon having different pore sizes and amount of porosity (active C, carbon nanotubes, C aerogels, C fibers mats, etc.) have been studied.^[21] Porous C-rich Si-based PDCs have been also investigated as a confinement material in S cathodes.^[22–24]

In this work, we studied the electrochemical performance of three different sulfur/PDC cathodes. For two of them sulfur is contained in PDCs aerogels belonging to the Si-O-C and Si-C-N systems, respectively, obtained via CO₂ supercritical drying^[9,25] while in the third one sulfur is confined in a mesoporous SiOC processed via the “polymeric spacer” method.^[26] The composite cathodes have been electrochemically characterized and their performances are discussed and related to the chemical composition and microstructure of the PDCs scaffold.

2. Experimental Section

2.1. Synthesis of PDC Aerogel

Synthesis of the PDC aerogels followed published procedures.^[16,25] Commercial polysiloxane (polyhydromethylsiloxane, PHMS, CAS: 63148-57-2, ABCR, Karlsruhe, Germany) and polysilazane (Durazane 1800 CAS: 503590-70-3, DurXtreme, Ulm, Germany) were chosen as precursors for the synthesis of Si-O-C and Si-C-N aerogels, respectively. Divinylbenzene (DVB, CAS: 1321-74-0, technical grade 80%, Sigma-Aldrich, Saint Louis, MO, USA) was used as crosslinker. Platinum divinyltetramethyldisiloxane complex in xylene (Karstedt’s catalyst, CAS: 68478-92-2), with Pt content of ≈2% (Sigma-Aldrich, Saint Louis, MO, USA) was further diluted to obtain a solution containing 0.1 wt% of catalyst. Cyclohexane (Carlo Erba, CAS: 110-82-7, Milano, Italy) was used as solvent. Crosslinking was obtained via hydrosilylation reactions between the Si-H bonds of the Si-polymer and the vinyl groups of DVB in the presence of Pt catalyst.^[27] The preceramic polymer (PHMS or Durazane) was mixed with DVB in cyclohexane and then Pt catalyst was added. The amounts of the reagents used for the synthesis are reported in **Table 1**. The mixture was magnetically stirred for 5 min and then poured into the Teflon container of a pressure reactor (Parr Digestion Vessel 4749, Parr Instrument Company, Moline, IL, USA). The reactor was then heated at 180 °C/24 h to complete the curing of the gel. At the end of the crosslinking process, the wet gel was solvent exchanged in cyclohexane (2 times a day for 3 days) before loading into the reactor for CO₂ supercritical drying. Preceramic aerogels were pyrolyzed at 1,000 °C/1 h, 10 °C min⁻¹, in flowing Ar (100 mL min⁻¹) using alumina boats in an alumina tube furnace (Lindberg Blu, USA).

2.2. Synthesis of Mesoporous SiOC

Synthesis of the mesoporous SiOC via the “polymeric spacer” method is reported in detail elsewhere.^[26] In this case, PHMS (CAS: 63148-57-2, ABCR, Karlsruhe, Germany) is reacted, via hydrosilylation reactions, with a vinyl-terminated polydimethylsiloxane having an average molecular weight of 9,400 DA, viscosity 200 cSt. (Vy-PDMS, CAS: 68083-19-2, Gelest, Morrisville, PA, USA) and with 1,3,5,7-tetravinyl-1,3,5,7-tetramethylcyclotetrasiloxane 95% (TVTMS, CAS: 27342-69-4, ABCR, Karlsruhe, Germany) used as crosslinker enhancer. The vinyl-terminated PDMS serves the double purpose of solvent, at the initial stage of the synthesis, and as a size-controlling templating agent. Indeed, during pyrolysis, vinyl-PDMS decomposes almost completely and leaves a porous SiOC with pore size related to its MW. Details of the synthesis are reported in Table 1. Mesoporous SiOC samples were obtained after pyrolysis at 800 °C/1 h using the same furnace and pyrolysis conditions (heating rate and atmosphere) as the PDC aerogels.

In both cases, for the synthesis of the aerogels and of the mesoporous SiOC, the manipulation of the reagents was performed under gentle Ar flow to prevent reaction with oxygen and moisture.

2.3. Preparation of the Porous PDC/S Composite Cathodes

To produce the composite electrodes, a recipe proposed by Qu et al.^[23] was followed. In brief, the porous SiOCs were first milled using a mortar to obtain fine powders and, after that, a quantity of sulfur doubled in weight with respect to the SiOC was added and the powders were further milled to homogenize the mixture. The SiOC/S powders were then loaded into a pressure reactor (Parr digestion vessel) which was placed inside an oven at 155 °C for 24 h. At these conditions, sulfur is in its liquid state and can flow into the pores of the ceramic matrix.

Once the thermal treatment was completed, the mixture was extracted from the vessel and grounded to obtain a composite powder which was further used to produce the electrodes for testing. Accordingly, a slurry containing 85 wt% PDC-sulfur composite, 10 wt% polyvinylidene fluoride, PVDF, as a binder, and 5% super P carbon black (Timcal Ltd) was prepared. Methyl-2-pyrrolidone (NMP, BASF) was utilized as a solvent of the slurry. Aluminum foil (Alfa Aesar) was employed as contact over which the slurry was pasted and consequently dried (in the oven, at 40 °C for 24 h). Electrodes of 10 mm diameter were punched out of the deposited material to serve as ready-to-use cathodes. Swagelok cells were assembled in a T-cell configuration,

Table 1. Amounts of reagents used in the synthesis of the preceramic samples.

Sample	Preceramic polymer	Crosslinker	DVB/Preceramic polymer [wt wt ⁻¹]	TVTMS/PHMS [wt wt ⁻¹]	Vinyl-PDMS/PHMS [wt wt ⁻¹]	Pt catalyst [μg^{-1} of preceramic polymer]	Cyclohexane [vol%]
SiOC-A	PHMS	DVB	2	–	–	200	90
SiCN-A	Durazane 1800	DVB	2	–	–	100	90
spSiOC	PHMS	TVTMS	–	0.04	1.5	20*	–

*Pt 2% (not diluted).

separating the cathode and a 0.75 mm thick lithium foil (anode) with an A-grade quartz membrane. As a liquid electrolyte, we utilized 1 M lithium bis(trifluoromethanesulfonyl) imide, LiTFSI, dissolved in a mixture of 1,3-dioxolane, DOL, and dimethoxymethane, DME, in a 1:1 volume ratio. To reduce shuttle effects in the testing of the cells, 0.1 M LiNO₃ was added to the electrolyte solution. A total of two tests per composite cathode were performed to check for reproducibility of the electrochemical measurements.

2.4. Characterization Techniques

Porosity, pore size distribution, and specific surface area (SSA) of the porous SiOC were investigated by recording N₂ adsorption and desorption isotherms. Experiments were carried out with an Autosorb iQ analyzer (Anton-Paar, Gratz, AU) in the 10⁻⁶ ≤ P/P⁰ ≤ 1 range. A nonlocal density functional theory (NLDFT) approach on the adsorption branch of the isotherm was utilized for the pore size distribution in the mesopore-micropore range, imposing an adsorption model that of silica with cylindrical pores. All calculations were made using the Quantachrome ASiQwin software.

A Gemini SUPRA 40 FE-SEM scanning electron microscope (Carl Zeiss, Germany) was used to investigate the morphology of the porous ceramic SiOC. Micrographs were obtained after sputtering the sample surface with an Au/C film to prevent charging during the observation.

Thermogravimetric and differential thermal analysis (TGA/DTA) measurements were performed using a Netzsch STA 409 instrument. The main objective of this measurement was to estimate the amount of sulfur in the composites. The thermal evolution of the aerogel-sulfur composites was carried out under 100 cc min⁻¹ pure air flow, heating about 50 mg of material with a 10 °C min⁻¹ rate up to a temperature of 1,000 °C.

C and Si contents of the ceramic samples were analyzed by Mikroanalytisches Labor Pascher (Remagen-Bandorf, Germany). Carbon was analyzed based on combustion techniques while silicon was measured using inductively coupled plasma atomic emission spectroscopy.

X-ray diffractograms, XRD, were collected using a Rigaku D-Max diffractometer (Rigaku, Tokyo, Japan) in the Bragg-Brentano configuration with CuK_α radiation operating at 40 kV and 30 mA. The scanning range was 2θ = 10–60 with a step rate of 0.05° and an acquisition time of 5 s per point.

The electrochemical performance was analyzed using galvanostatic cycling with potential limitation (GCPL) on VMP-multipotentiostat (Biologic Science Instruments, France) and controlled constant temperature of 25 °C. Cells were cycled by GCPL in a potential range of 1.2–3.6 V with a current of 83.5 mA g⁻¹. For electrodes fabrication, 85 wt% SiCN-S composite as active material, 10 wt% polyvinylidene fluoride (PVDF) as binder, and 5 wt% carbon black (Super P, Timcal Ltd, Switzerland) as conduction additive were mixed with N-Methyl-2-pyrrolidone (NMP, BASF, Germany) to form slurry. Then the slurry was pasted onto an aluminum foil by a doctor blade and then dried at 40 °C in the oven for 24 h until NMP completely evaporated. After cutting and then drying in a Büchi glass oven (Labortechnik AG, Germany) for 24 h, electrodes with 10 mm of diameter were obtained. Afterward,

Swagelok cells were assembled in an argon-filled glove box without air contact. Lithium foil (0.75 mm thickness, Alfa Aesar, Germany) was used as the counter and QMA (Whatmann, UK) as separator. Electrolyte contained 1 M lithium bis(trifluoromethanesulfonyl) imide (LiTFSI) dissolved in a mixture of 1,3-dioxolane (DOL) and dimethoxymethane (DME) with a volume ratio 1:1. Besides, 0.1 M of LiNO₃ was added into the electrolyte to alleviate the shuttle effect.

Galvanostatic charge/discharge measurements were performed at a low rate of C/20, corresponding to a current of 83.5 mA per gram of sulfur (the specific capacity of the active material was assumed to be 1,670 mAh g⁻¹). The potential range of the measurement was fixed between 1.2 and 3.6 V. The charge/discharge profiles were built point by point knowing the voltage and the inserted/extracted charge capacity. The total specific capacity refers to the total electrode mass. Furthermore, the coulombic efficiency was calculated as the ratio between delithiation (charge) and lithiation (discharge) capacities.

Extended cycling stability was evaluated either by repeating the galvanostatic charge/discharge measurements for 100 cycles at C/20 rate and by increasing, after five cycles, the rate from C/20 to C/10, C/5, C/2, and C and then by repeating the test at C/20 rate. Finally, cyclic voltammetry was performed to assess the nature of redox reactions occurring in the PDC-derived Li-S batteries by imposing scan rates of 0.02 mV s⁻¹.

The electrochemical impedance spectroscopy (EIS) was obtained also by VMP-multipotentiostat (Biologic Science Instruments, France) at a voltage of 10 mV from 100 kHz to 10 mHz at room temperature.

3. Result and Discussion

3.1. Characterization of the Porous Ceramics before and after Sulfur Infiltration

Figure 1 reports the adsorption/desorption isotherms and the corresponding pore size distribution curves recorded on the starting porous samples before sulfur infiltration. SiOC-A and SiCN-A show type IV and type II isotherms, respectively, SiOC-A having a clear H1 hysteresis loop.^[28] Compared to SiOC-A, SiCN-A shows a lower total porosity volume (0.15 vs 0.60 cm³ g⁻¹), and the hysteresis is shifted to higher relative pressure due to the formation of large mesopores/macropores. The pore size distribution curves (Figure 1b) confirm that SiCN-A has pores larger than SiOC-A (ca 70 vs 20 nm). The adsorption/desorption isotherm of the mesoporous spSiOC sample is of type IV with H2 hysteresis loop, revealing that the mesopores have an ink-bottle shape. In this case, the total porosity is 0.32 cm³ g⁻¹ and the pore size distribution curve, obtained from the adsorption branch of the isotherm, shows two maxima, one in the micropore range (ca 1 nm) and the other in the mesopore regime at 6 nm. The specific surface area (SSA) of the three types of porous ceramics follows a trend closely related to their pore size distribution: spSiOC, which presents a fine porosity spanning between 1 and 10 nm, is characterized by an SSA of 455 m² g⁻¹; on the contrary, SiCN-A has a low SSA of 46 m² g⁻¹ due to its macroporous characteristic. Finally, SiOC-A aerogels present an SSA of 161 m² g⁻¹ in accordance with

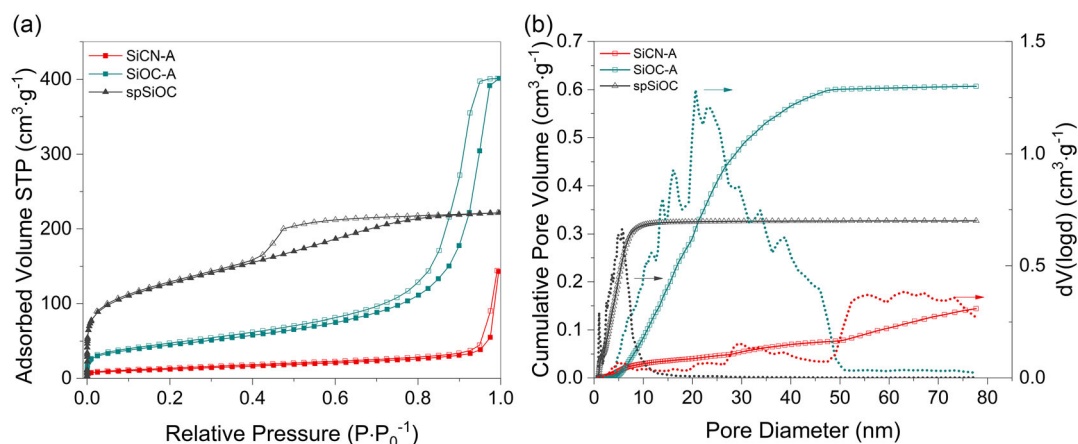


Figure 1. a) N₂ physisorption isotherms and b) DFT pore size distributions recorded on the porous ceramics before the sulfur infiltration.

Table 2. Results from the Ads/Des analysis of the three porous PDCs.

Sample	Isotherm	Hysteresis loop	SSA [m ² ·g ⁻¹]	DFT pore volume [cc·g ⁻¹]	Pore size [nm]
SiOC-A	Type IV	H1	161	0.60	20
SiCN-A	Type II	–	46	0.15	70
spSiOC	Type IV	H2	455	0.32	1 and 6

its intermediate values of pore size distribution. Details of the results obtained from the N₂ adsorption/desorption analysis are reported in **Table 2**.

SEM pictures of the fracture surfaces of the porous samples help in characterizing the nanostructure of the ceramic scaffolds (**Figure 2**). Accordingly, the two aerogel samples are both formed by colloidal particles, as is typical for these materials.^[9] SiOC-A sample shows finer individual particles and smaller pore size compared to the SiCN-A one. From the SEM picture taken at the highest magnification (**Figure 2**, top right), the particle size

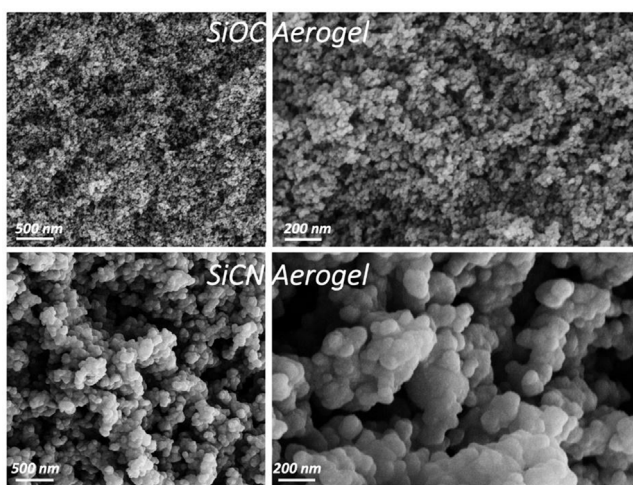


Figure 2. SEM picture showing the nanostructure of the ceramic aerogels: SiOC (top) and SiCN (bottom).

for SiOC-A can be estimated in the range of a few tens of nanometers while for SiCN-A sample (**Figure 2**, bottom right) particles of a hundred (or more) nm can easily be found. Likewise, pore sizes of SiCN aerogel can reach several hundred of nanometers. For both aerogels and specifically for SiCN-A, SEM demonstrates the presence of macropores (pore size > 50 nm, according to IUPAC definition), implying that the total pore volume estimated from the N₂ sorption analysis is probably underestimated, in particular for SiCN-A.

SEM acquisitions on the mesoporous spSiOC ceramic (**Figure 3**) reveal only a rough surface, in agreement with the very fine porosity of this sample disclosed by the N₂ sorption analysis. No macropores have been seen in this sample and accordingly, the pore volume extracted from the N₂ analysis (0.32 cm³·g⁻¹) should be very close to the total actual pore volume.

As reported in many studies, the amorphous polymer-derived, Si-based ceramic network contains a free carbon phase that controls many functional properties, including electrical conductivity.^[29,30] It is therefore important, for the application envisaged in this study, to quantify the amount of free C which correlates, as a first approximation, to the electrical conductivity.^[31] The amount of free carbon can be estimated by performing a TGA in air-flow.^[32] The weight loss, measured in the temperature range 400–700 °C, is associated with the reaction C + O₂ → CO₂ and it is therefore a direct measure of the amount of free C present in the ceramic. TGA curves of the three porous samples before sulfur infiltration are shown in **Figure 4a**. The two

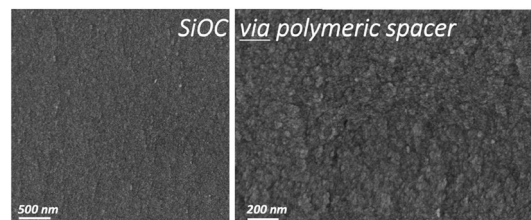


Figure 3. SEM of the fracture surface of the mesoporous SiOC obtained via “polymeric spacer.” Porosity is indirectly observed from the roughness of the fracture surface which is clearly seen in the picture at the highest magnification (150.000 X).

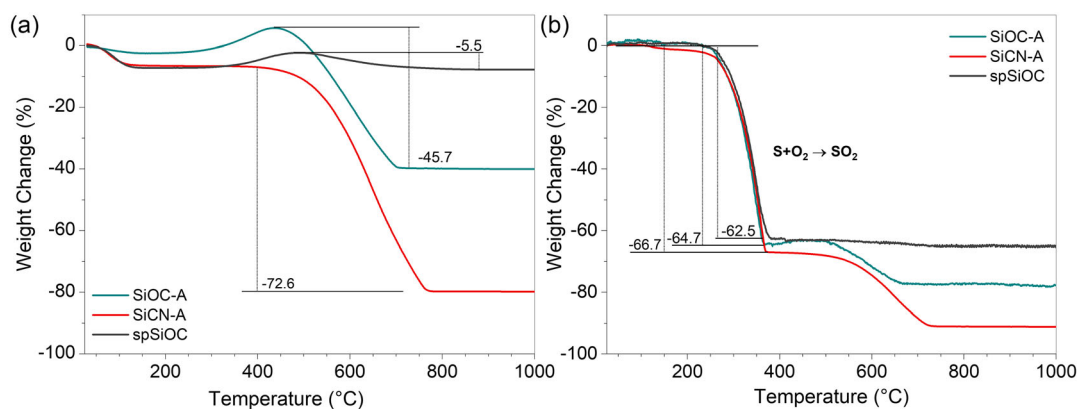


Figure 4. TGA curves recorded in airflow on the porous ceramics a) before and b) after sulfur infiltration.

aerogels, SiOC-A and SiCN-A, show a weight loss of 45.7 and 72.6%, respectively, which correspond to the amount of free C in the two systems. Mesoporous spSiOC has a lower amount of free C being the weight loss, in this case, of only 5.5% (Table 3). The TGA curves of the two SiOC systems show also an additional small weight increase before the free C oxidation, in the temperature range 350–450 °C. Such a thermogravimetric effect has been already reported in the literature and is generally explained by the oxidation of Si-CH_x groups, which leads to Si-O-Si bonds, accordingly, explaining the weight increase.^[33,34] Thermogravimetric curves recorded in flowing air for the three sulfur/PDC composites are shown in Figure 4b. The curves show a steep weight loss within 62% and 67% in the temperature range 200–400 °C which is due to the oxidation of S to SO₂ and demonstrate that the sulfur content of the PDC/S composites is very close to the expected one (Table 4). Then, the weight loss step from ≈500 to ≈700 °C is assigned to the oxidation of free C and agrees quite well with the value of C_{free} previously estimated. Chemical analyses of the carbon and silicon fractions in neat

Table 3. TGA measured amounts of C_{free} (wt%) in the porous PDCs. Chemical analyses of carbon and silicon fractions in the neat ceramic samples are given, too.

Sample	Thermogravimetry	Chemical analysis	
	C _{free} [wt%]	C [wt%]	Si [wt%]
SiOC-A	45.7	43.6 ± 0.4	26.1 ± 0.0
SiCN-A	72.6	68.60 ± 0.9	9.5 ± 0.1
spSiOC	5.5	14.8 ± 0.1	42.4 ± 0.1

Table 4. TGA measured amounts of infiltrated S (wt%) in the PDC/S composites.

Sample	Thermogravimetry	
	C _{free} [wt%]	S [wt%]
SiOC-A/S	–	64.7
SiCN-A/S	–	66.7
spSiOC/S	–	62.5

ceramic aerogels are given in Table 3. Here, for the SiOC-A and SiCN-A carbon is lower at around 2–3 wt% when compared with previous data. For the spSiOC sample, C_{free} measured by TGA is lower compared to the total C provided via chemical analysis, suggesting that, for this sample, most of the C is bonded to the network via Si-C bonds.

X-ray diffraction analysis demonstrates the amorphous character of the PDC scaffold, and after sulfur infiltration, XRD confirms the presence of crystalline S₈ (Figure S1, Supporting Information).

3.2. Electrochemical Performances of the PDCs Cathodes

Galvanostatic cycling with potential limitation (GCPL) tests were first run in a discharge configuration, with the as-prepared cathodes already filled with nonlithiated sulfur. First lithiation and delithiation profiles are depicted in Figure 5, where it is evident that SiOC-A-derived cathodes perform better than SiCN and spSiOC in terms of initial specific capacity. As a matter of fact, the first discharge of the SiOC-A cathode shows a capacity of 909 mAh g⁻¹, while those of the SiCN-A and spSiOC cathodes give a value of ≈704 and 671 mAh g⁻¹, respectively. Clear lithiation plateaus are visible in all kinds of cathodes at around 2.3 and 2.0 V, these occurring as a consequence of the formation of high-order soluble polysulfides (e.g., Li₂S₈, Li₂S₄) and low-order solid polysulfides (e.g., Li₂S₂).^[35] The final steep potential loss is ascribable to the conversion into solid Li₂S, where the cathode is considered discharged. The following charge ends up with specific capacities of 837, 565, and 610 mAh g⁻¹, for SiOC-A, SiCN-A, and spSiOC, respectively. A consistent loss in specific capacity is nevertheless observed in all cases, suggesting a dissolution of polysulfides in the electrolyte during the first lithiation.

Extended cycling stability was defined with an imposed C/20 rate in the 1–100 cycles range and relative results are given in Figure 6a. As a first comment, it is clear that a consistent loss of capacity occurs in all the PDC cathodes, showing a stabilization of the specific capacity with the ongoing measurement. After 100 cycles, the SiOC-A, SiCN-A, and spSiOC cathodes retain 112, 62, and 126 mAh g⁻¹, respectively, corresponding to a total retention of 12%, 9%, and 19%, respectively, of the initial capacity. Some information on the shuttle effect can be retrieved from

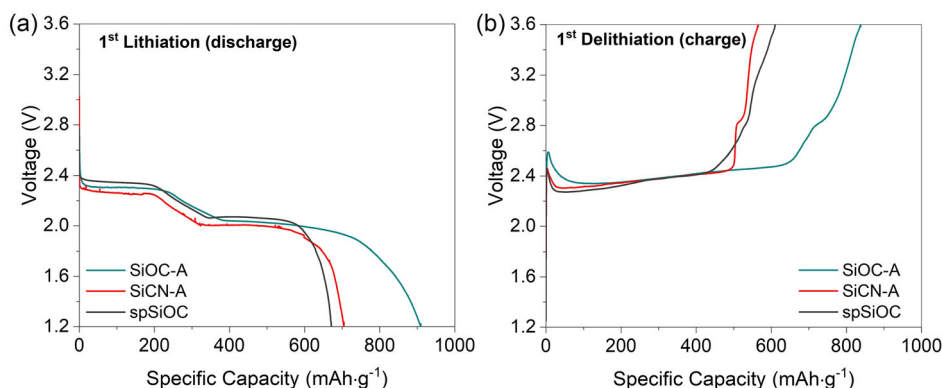


Figure 5. Galvanostatic discharge/charge curves of SiOC-A, SiCN-A, and spSiOC-based cathodes during: a) lithiation corresponding to the first discharge of the Li-S cell and b) first delithiation (first charge of the Li-S cell).

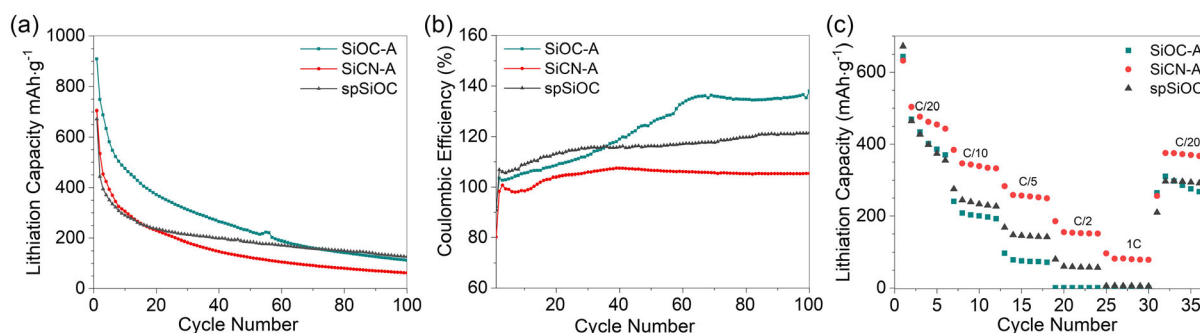


Figure 6. a) Extended constant rate cyclic stability, b) coulombic efficiency in the 2-100 cycles range, and c) variable rate cycling of the two prepared cathodes.

the extended cycling stability by plotting the cycle-by-cycle coulombic efficiency. As a matter of fact, it has been demonstrated that efficiencies outbreaking 100% are observed when soluble polysulfides are shuttled toward the anode, where sulfur oxidation releases the excess charge responsible for the efficiency boost.^[22,23]

We report the coulombic efficiency of SiOC-A, SiCN-A, and spSiOC in Figure 6b. Evidently, silicon oxycarbide-based cathodes show an increase in the efficiency toward 140% and 120% for the SiOC-A and spSiOC, respectively, which remain stable from the 60th and 30th cycle on, respectively. The reason for the efficiency over 100% is an increasing degree of shuttling effect. Namely, the long-chain polysulfides migrate to the Li anode, are chemically reduced, diffuse back to the cathode, and are further oxidized to a long-chain polysulfide, leading to a long charge (delithiation) process with efficiency losses. The shuttling phenomenon does not appear to largely affect the potential/capacity transient of SiCN-A cathode. From here, we could derive a hypothesis on the effect of the chemical composition of the scaffold material being the SiCN more suitable to hinder the shuttle phenomena than SiOC. As a matter of fact, it is known that nitrogen-containing cathodes are able to strongly chemisorb polysulfides at the nitrogen sites, so the shuttling effect is largely hindered.^[36] This also signifies that the chemical composition of a matrix material may be advantageous over the present porosity. On the other side, the better electrochemical performance of

spSiOC compared to SiOC-A could be related to its smaller pore size and to its ink-bottle shape which, evidently, can more efficiently hamper the shuttle behavior compared to the larger mesopores present in SiOC-A. Similar pore size effects have been observed in a recent work, where microporosity is addressed as a major factor in limiting shuttling phenomena compared with mesoporosity, in hierarchical porous carbon nanoparticles.^[24]

Figure 6c displays the variable rate cycling of the cathodes, where the SiCN-A cathode shows superior charge/discharge ability at fast charging/discharging rates. The rate performance is primarily determined by the ionic and electronic conductivity of the matrix material. High free carbon content leads to higher electrical conductivity of SiCN-A sample, thus providing pathways for better transport of ions and electrons and enhanced performance of this material at high-rate charge/discharge tests. In contrast, the slightly better performance of the spSiOC compared to SiOC-A at high rates is more difficult to explain, indeed, the same two parameters (free C content and pore size) should suggest an opposite trend. A possible explanation might reside in the large SSA of this material, which might be beneficial for fast Li⁺ adsorption directly at the contact interface.

Finally, cyclic voltammetry was employed as an analytical method to define the ability of the cathodes to withstand cyclability from an electrochemical point of view, investigating the nature of redox reactions occurring at their interface.

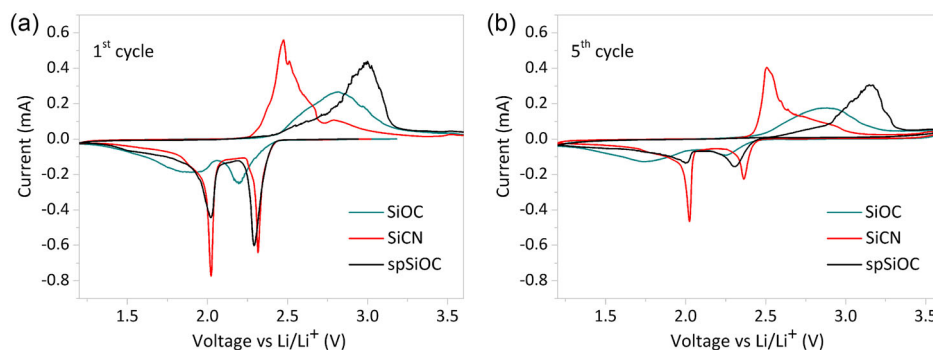


Figure 7. Cyclic voltammetry of the a) first and b) fifth cycles of the sulfur-containing PDC cathodes.

Figure 7a,b reports the first and fifth voltammetric cycles, respectively. As a reference point, positive current refers to the sulfur oxidation reaction (charge), and negative current to the reduction one (discharge). The first cathodic (discharge) peak appears at 2.3 V corresponding to the conversion of S_8 to high-order polysulfides (Li_2S_x , $4 < x < 8$). The second cathodic peak appears at 2.0 V and corresponds to the further reduction of polysulfides to insoluble Li_2S_2 and Li_2S . During the oxidation process, a main anodic peak should appear at 2.4 V, attributed to the conversion of lithium sulfide to S_8 . Usually, it consists of the overlap of two peaks corresponding to oxidation of the species reduced within two cathodic peaks. For SiCN-A both oxidation and reduction peaks are quite sharp, and the distance between them is the lowest among all the investigated materials. This signifies that SiCN-A presents the lowest ohmic losses, attributed to a high carbon content providing a good electrical conductivity. Cathodic and anodic peaks registered for SiOC-A are much broader and significantly shifted toward negative (around 100 mV) and positive (around 400 mV) direction, respectively. This signifies a much higher polarization related to the ohmic drop compared with the one of SiCN-A. This feature can be attributed to a lower amount of free carbon, leading to a lower conductivity. The broad peaks can also be correlated to dissolution and diffusion of polysulfides, which is boosted for this material (compare Figure 6b).

The CV curve registered for spSiOC is quite atypical. While cathodic peaks almost superimpose with those of SiCN-A, the anodic peak is shifted significantly into the positive direction (>600 mV). According to literature reports,^[37] this feature can be attributed to the presence of a high amount of long-chain polysulfides which delithiate first at higher potentials.

In spSiOC, the rather high SSA and ordered pore structure might also trigger a pseudocapacitive response of the cathode.^[38] Such behavior emerges when charged ions are mainly adsorbed onto the surface of the material, rather than in its bulk.^[39] If we consider that spSiOC is provided with a smaller amount of carbon compared to other aerogels, but with a much higher SSA, its sharp peaks in the cyclic voltammetry might be indicative of surface adsorption. This especially holds when considering that for ultramicroporous materials with very fine porosity, it is not possible to discriminate the bulk of the solid from its surface, and this applies also to sulfur dispersed in such a fine matrix. Likewise, if we consider the rate capacity measurements, the spSiOC scaffold presents smaller drops in the capacity compared to the other SiOC aerogel, a behavior that might be predominantly ascribed to surface adsorption, instead of Li^+ migration toward the bulk of sulfur.

Table 5 shows the comparison of electrochemical performances of silicon-based positive LIS electrodes that can be compared with the result presented in this article. As a matter of fact, the overall capacity and stability of Si-based scaffolds for Li-S batteries seem to be promising when synthesizing SiC, SiOC, or SiCN with nanostructured features presenting large fractions of carbon and not necessarily large SSAs. Compared to this work, optimized reversible capacities have been reported to outreach 500 mAh g^{-1} even after 400 cycles, suggesting that polymer-derived ceramic aerogels might be engineered to boost their performances. Compared to other electrode materials, ceramic aerogels have the advantage of being able to accommodate large volume variations thanks to their solid colloidal structure, thus partially solving the issues related to sulfur expansion.

Table 5. Comparative table of electrochemical performances of similar cathode materials for Li-S battery storage.

Sulfur host material	Sulfur content [wt%]	SSA [$\text{m}^2 \text{g}^{-1}$]	Initial capacity [mAh g^{-1}]	Reversible capacity [mAh g^{-1}]	Number of cycles	References
SiOC-A/S	64.7	161	909	112	100	This work
SiCN-A/S	66.7	46	704	62	100	This work
spSiOC/S	62.5	455	671	126	100	This work
HPCN11	76	2789	1129	590	400	[24]
SiCN-S-1000	66.6	72	722	313	40	[23]
SiOCN-5/S-CP	70	38.2	1015	374	500	[40]
S-CNTs/SiC	75.6	61.6	1008	316	400	[41]

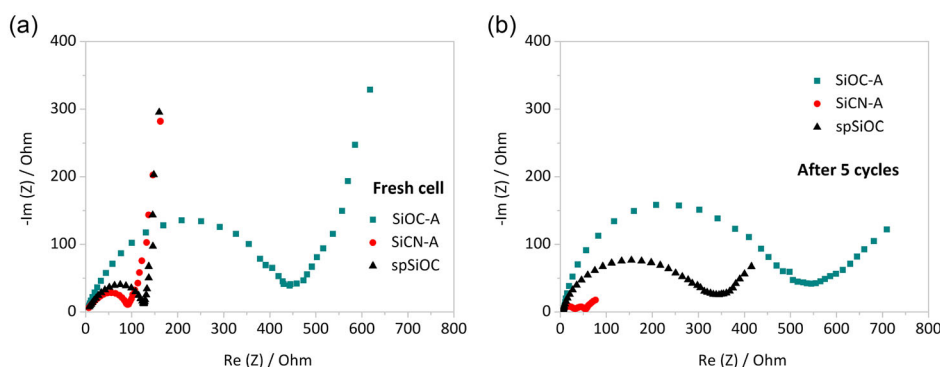


Figure 8. Nyquist plots of all samples a) before and b) after five cycles.

The electrochemical impedance spectroscopy (EIS) measurements were performed on the freshly assembled cell after five cycles (**Figure 8**). The diameter of the semicircle at the high-frequency region is attributed to the charge-transfer resistance (R_{ct}) of the material and the slope of the spectrum at the low frequencies is associated with the electrolyte resistance (R_e). The equivalent circuit of the lithium-sulfur battery is shown in **Figure 9** and all resistance values of the samples before and after five cycles are listed in **Table 6**. Before electrochemical cycling, the diameters of the semicircle of SiCN-A and spSiOC are much smaller than SiOC-A. Especially for SiCN-A, the value of R_{ct} of it is 100.3 Ohm, the lowest charge-transfer resistance compared to other samples. After five cycles, the charge-transfer resistance of SiOC-A and spSiOC increases to 464 Ohm and 289.8 Ohm from 460.5 and 127.8 Ohm, respectively, which is indicated by bigger corresponding semicircles and the spectra fitting results. Besides, the increased R_e of SiOC-A to 5.498 Ohm reveals a higher ions diffusion resistance of the electrolyte. However, for SiCN-A, not only the ion diffusion resistance decreases to almost 0, but also the charge-transfer resistance within the electrode diminishes significantly to

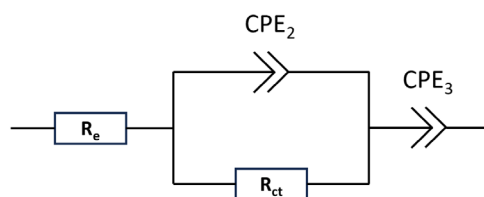


Figure 9. The equivalent circuits of the battery. R_e is associated with the resistance of the electrolyte, R_{ct} represents the charge transfer resistances, and CPE_2 and CPE_3 are the constant phase elements.

Table 6. Resistance list of all samples. R_e and R_{ct} represent the resistance of electrolytes and the charge transfer before cycling. R_e' and R_{ct}' represent the resistance of the electrolyte and the charge transfer after five cycles.

	R_e [Ohm]	R_{ct} [Ohm]	R_e' [Ohm]	R_{ct}' [Ohm]
SiOC-A/S	2.221	460.5	5.498	464
SiCN-A/S	2.438	100.3	≈0	22.95
spSiOC/S	3.611	127.8	2.99	289.8

22.95 Ohm. We attribute this behavior to a better distribution of sulfur in big pores of SiCN-A being a consequence of cycling and the sulfur volume changes related to this process. Elemental analysis results have also shown that SiCN-A contains the highest amount of carbon, thus the sulfur volume changes during cycling possibly causing also a rearrangement of a free carbon phase leading to a higher conductivity. Moreover, the low charge transfer resistance probably enables the good rate capability of the materials, as shown in **Figure 6c**.

4. Conclusion

In conclusion to this work, polymer-derived ceramic SiOC and SiCN aerogels were successfully synthesized and utilized as scaffolds for sulfur containment in Li-S batteries. Their electrochemical performances were studied together with those of a porous SiOC ceramic with a peculiar ink bottle-shaped fine mesoporosity obtained via selective degradation of molecular spacers. Results show that despite the impressive initial capacities shown by all of the scaffolds, SiOC and SiCN materials present capacities fading toward the 110–60 mAh g⁻¹ range, losing around 90% of their first specific capacity. Despite the smaller pore volume, SiCN-A possesses a major fraction of free carbon as compared to the other scaffolds, which eventually guarantees good electrical conductivity, and the presence of nitrogen in the ceramic network further retains the efficiency toward chemisorption of a fraction of polysulfides.

For what concerns SiOC scaffolds, results indicate that a fine porosity (1–10 nm wide) might be the key for partially hinder shuttling phenomena in Si-based compounds. As a matter of fact, large mesopores of SiOC-A (≈20 nm) can be associated with severe shuttling and efficiency losses, while fine pores of spSiOC result in a damped degradation and faster charge/discharge abilities.

Further studies concerning the use of microporous PDCs with ink bottle-shaped pores will clarify whether these might result in a better retainment of the initial capacity of these novel Li-S cathodes.

Supporting Information

Supporting Information is available from the Wiley Online Library or from the author.

Acknowledgements

A.Z. and Gian G.D.S. acknowledge the financial support by the Italian Ministry of University and Research (MIUR) within the program PRIN2017 - 2017PMR932 "Nanostructured Porous Ceramics for Environmental and Energy Applications". F.Q. acknowledges the financial support from the China Scholarship Council (CSC, No. 201904910776). Open access funding enabled and organized by Projekt DEAL.

Conflict of Interest

The authors declare no conflict of interest.

Data Availability Statement

The data that support the findings of this study are available on request from the corresponding author. The data are not publicly available due to privacy or ethical restrictions.

Keywords

aerogels, Li-S batteries, lithium, polymer-derived ceramics, porous ceramics, sulfur

Received: May 5, 2023

Revised: August 6, 2023

Published online: October 2, 2023

-
- [1] S. Yajima, J. Hayashi, M. Otori, *Chem. Lett.* **1975**, 4, 931.
- [2] P. Colombo, G. Mera, R. Riedel, G. D. Sorarù, *J. Am. Ceram. Soc.* **2010**, 93, 1805.
- [3] A. Viard, D. Fonblanc, D. Lopez-Ferber, M. Schmidt, A. Lale, C. Durif, M. Balestrat, F. Rossignol, M. Weinmann, R. Riedel, S. Bernard, *Adv. Eng. Mater.* **2018**, 20, 1800360, .
- [4] A. L. Hector, *Coord. Chem. Rev.* **2016**, 323, 120.
- [5] H. Ichikawa, *Annu. Rev. Mater. Res.* **2016**, 46, 335.
- [6] P. Colombo, *J. Eur. Ceram. Soc.* **2008**, 28, 1389.
- [7] E. Zera, R. Camprostrini, P. R. Aravind, Y. Blum, G. D. Sorarù, *Adv. Eng. Mater.* **2014**, 16, 814.
- [8] Z. C. Eckel, C. Zhou, J. H. Martin, A. J. Jacobsen, W. B. Carter, T. A. Schaedler, *Science (80-)*. **2016**, 351, 58.
- [9] G. D. Sorarù, E. Zera, R. Camprostrini, *Handbook of Sol-Gel Science and Technology* **2016**, <https://doi.org/10.1007/978-3-319-19454-7>.
- [10] S. Aguirre-Medel, P. Jana, P. Kroll, G. D. Sorarù, *Materials* **2018**, 11, 2589 .
- [11] A. Zambotti, F. Valentini, E. Lodi, A. Pegoretti, V. Tyrpekl, S. Kohúteková, G. D. Sorarù, M. Kloda, M. Biesuz, *J. Alloys Compd.* **2021**, 895, 162592.
- [12] A. Zambotti, E. Caldesi, M. Pellizzari, F. Valentini, A. Pegoretti, A. Dorigato, G. Speranza, K. Chen, M. Bortolotti, G. D. Sorarù, M. Biesuz, *J. Eur. Ceram. Soc.* **2021**, 41, 5484.
- [13] M. C. Bruzzoniti, M. Appendini, B. Onida, M. Castiglioni, M. D. Bubba, L. Vanzetti, P. Jana, G. D. Sorarù, L. Rivoira, *Environ. Sci. Pollut. Res.* **2018**, 25, 10619.
- [14] A. Zambotti, A. Bruni, M. Biesuz, G. D. Sorarù, L. Rivoira, M. Castiglioni, B. Onida, M. C. Bruzzoniti, *SSRN Electron J.* **2023**, 11, 109771.
- [15] H. Fukui, H. Ohsuka, T. Hino, K. Kanamura, *ACS Appl. Mater. Interfaces.* **2010**, 2, 999.
- [16] P. Vallachira Warriam Sasikumar, E. Zera, M. Graczyk-Zajac, R. Riedel, G. D. Soraru, B. Dunn, *J. Am. Ceram. Soc.* **2016**, 99, 2977.
- [17] M. Li, J. Lu, Z. Chen, K. Amine, *Adv. Mater.* **2018**, 30, 1800561.
- [18] G. E. Blomgren, *J. Electrochem. Soc.* **2017**, 164, A5019.
- [19] Y. X. Yin, S. Xin, Y. G. Guo, L. J. Wan, *Angew. Chem., Int. Ed.* **2013**, 52, 13186.
- [20] A. Eftekhari, D. W. Kim, *J. Mater. Chem. A* **2017**, 5, 17734.
- [21] J. Chai, J. Du, Q. Li, N. Han, W. Zhang, B. Tang, *Energy Fuels.* **2021**, 35, 15455.
- [22] F. Qu, Z. Yu, M. Krol, N. Chai, R. Riedel, M. Graczyk-Zajac, *Nanomaterials* **2022**, 12, 1283.
- [23] F. Qu, M. Graczyk-Zajac, D. Vrankovic, N. Chai, Z. Yu, R. Riedel, *Electrochim. Acta.* **2021**, 384, 138265.
- [24] S. Eun, M. Ji, J. Park, J. W. Lee, D. W. Yoon, Y. Kim, J. H. Kim, Y. C. Kang, D. S. Jung, *Chem. Eng. J.* **2023**, 465, 143035.
- [25] V. L. Nguyen, E. Zera, A. Perolo, R. Camprostrini, W. Li, G. D. Sorarù, *J. Eur. Ceram. Soc.* **2015**, 35, 3295.
- [26] Y. Blum, G. D. Sorarù, A. P. Ramaswamy, D. Hui, S. M. Carturan, *J. Am. Ceram. Soc.* **2013**, 96, 2785.
- [27] Y. D. Blum, D. B. MacQueen, H. J. Kleebe, *J. Eur. Ceram. Soc.* **2005**, 25, 143.
- [28] F. Rouquerol, J. Rouquerol, K. S. W. Sing, P. Llewellyn, G. Maurin, *Adsorption by Powders and Porous Solids*, Academic Press **2014**.
- [29] Q. Wen, Z. Yu, R. Riedel, *Prog. Mater. Sci.* **2020**, 109, 100623.
- [30] F. Dalcanele, J. Grossenbacher, G. Blugan, M. R. Gullo, A. Lauria, J. Brugger, H. Tevaearai, T. Graule, M. Niederberger, J. Kuebler, *J. Eur. Ceram. Soc.* **2014**, 34, 3559.
- [31] J. Kaspar, M. Graczyk-Zajac, S. Choudhury, R. Riedel, *Electrochim. Acta.* **2016**, 216, 196.
- [32] M. Graczyk-Zajac, D. Vrankovic, P. Waleska, C. Hess, P. V. Sasikumar, S. Lauterbach, H.-J. Kleebe, G. D. Sorarù, *J. Mater. Chem. A* **2018**, 6, 93.
- [33] M. Narisawa, K. Terauds, R. Raj, Y. Kawamoto, T. Matsui, A. Iwase, *Scr. Mater.* **2013**, 69, 602.
- [34] G. D. Sorarù, C. Tavonatti, L. Kundanati, N. Pugno, M. Biesuz, *J. Am. Ceram. Soc.* **2020**, 103, 6519.
- [35] X. Zhang, H. Xie, C.-S. Kim, K. Zaghib, A. Mauger, C. M. Julien, *Mater. Sci. Eng. R: Rep.* **2017**, 121, 1.
- [36] J. Song, M. L. Gordin, T. Xu, S. Chen, Z. Yu, H. Sohn, J. Lu, Y. Ren, Y. Duan, D. Wang, *Angew. Chem.,– Int. Ed.* **2015**, 54, 4325.
- [37] X. Huang, Z. Wang, R. Knibbe, B. Luo, S. A. Ahad, D. Sun, L. Wang, *Energy Technol.* **2019**, 7, 1801001.
- [38] M. Mastragostino, F. Soavi, C. Arbizzani, *Adv. Lithium-Ion Batter.* **2002**, 481, https://doi.org/10.1007/0-306-47508-1_17.
- [39] K. Brezesinski, J. Wang, J. Haetge, C. Reitz, S. O. Steinmueller, S. H. Tolbert, B. M. Smarsly, B. Dunn, T. Brezesinski, *J. Am. Chem. Soc.* **2010**, 132, 6982.
- [40] J. Q. Lu, J. L. Hu, H. X. Zhong, Y. L. Ren, L. Z. Zhang, *J. Alloys Compd.* **2021**, 860, 157903.
- [41] J. Y. Wang, W. J. Wang, H. P. Li, T. Z. Tan, X. Wang, Y. Zhao, *J. Nanopart. Res.* **2019**, 21, 113.